

Formation and dynamics of water clusters on Ru(001)

Y. Lilach,^{a)} V. Buch,^{b)} and M. Asscher^{c)}

Department of Physical Chemistry, The Hebrew University of Jerusalem, Jerusalem 91904, Israel

(Received 18 February 2003; accepted 16 September 2003)

The adsorption kinetics of water on Ru(001) was simulated using molecular dynamics (MD) and equilibrium-model approach. The results nicely reproduce observations from STM imaging, work function change, and IR measurements. The agreement with experimental results is based on the formation of stable clusters already at very low surface coverage and temperature. Tetramers are predicted to be relatively stable compared to smaller and larger clusters. The dipole moment per water molecule continuously decreases from 2.2D for the monomer down to 1.1D for pentamer and larger clusters. Dimers are found to diffuse faster than monomers or larger clusters, with activation energy for diffusion of 2.9 kcal/mol, in agreement with recent STM measurements. A unique mechanism for dimers diffusion is proposed. Temperature programmed desorption (TPD) spectra from a metal surface were calculated by employing the MD scheme. These spectra were found identical to the standard Redhead line-shape analysis of the experimental TPD spectra of water from Pt(111) and Ru(001), an observation that was used to verify the consistency of the MD procedure. Finally, a kinetic model, fed by the MD calculated decreasing dipole moments per water molecule at larger clusters, explains well the highly nonlinear initial stages (up to 0.35BL) of the work function change data determined experimentally. © 2003 American Institute of Physics.
[DOI: 10.1063/1.1625645]

I. INTRODUCTION

The adsorption and interaction of water on surfaces has been at the focus of interest for decades.^{1,2} New phenomena, however, keep emerging due to improved experimental tools^{3–8} which lead to better understanding of previously reported observations.³ The interaction and kinetics of water adsorption and desorption on Ru(001) and Pt(111) are relatively well understood since these systems received particular attention. The first water layers form a hexagonal bilayer (BL) structure on hexagonal metallic surfaces,⁹ following the Bernal–Fowler–Pauling^{10,11} rules for ice layer formation. Ice structure dictates that the second layer oxygen atoms should reside 0.96 Å above the first. However, careful IV-low energy electron diffraction measurements^{12,13} have led to the conclusion that the second H₂O layer is only 0.1 Å above the first layer (flattening is most likely due to interaction of the second layer with the metal). Another conclusion was that while D₂O forms a perfect bilayer structure, H₂O forms striped domains on the surface. Temperature programmed desorption (TPD) spectra of H₂O and D₂O from Ru(001) reveal a unique isotope effect. While for H₂O two peaks are present at 185 K (*A*₂) and 215 K (*A*₁), the second peak is practically nonexistent in the D₂O spectra.¹⁴ Whether these two isotope effects are correlated is still not fully resolved. Another factor that needs to be considered is H₂O and D₂O dissociation on the surface. TPD studies suggest that about 10% (surface quality dependent) of the first BL of H₂O dissociate upon heating to 200 K,^{13,15} but D₂O does not disso-

ciate. On the other hand, recent DFT¹⁶ calculations suggested that water interaction on Ru(001) can be described via dissociation of 50% of the adsorbed bilayer.

While very extensive literature is available on gaseous water clusters,^{17–22} the information regarding adsorbed clusters is much more limited.²³ Mitsui *et al.* have studied the formation of water clusters on Pd(111) by STM, and produced movies demonstrating their surface mobility.⁴ A cyclic (H₂O)₆, the basic building block of *I*_h ice, was observed.^{4,5} Nakamura *et al.* have studied H₂O/Ru(001) and H₂O/Pt(111)⁶ by infrared spectroscopy, claiming that monomers and tetramers are the most stable clusters on ruthenium at low coverages.⁶ Helium scattering studies⁷ suggest the dominance of dimers and trimers on Pt(111) below 100 K.

II. RESULTS AND DISCUSSION

In Sec. II A we shall introduce the molecular dynamics (MD) simulations as a model to describe the growth of water molecules via cluster formation on top of metallic substrates. Comparison of MD-TPD, performed here for the first time, to standard Redhead-type line-shape analysis of experimental TPD is then used to verify the validity of this theoretical tool in order to describe the water–metal system. The computed dipole moments per water molecule in the different clusters are then utilized as an input in a kinetic model (Sec. II B) that describes the experimental work function change data versus coverage.

A. Molecular dynamics simulations

Molecular dynamics simulations, based on model potential energy surfaces, were conducted in order to follow the initial adsorption, clustering, diffusion, and desorption of water molecules from platinum and ruthenium surfaces. After

^{a)}Also at The Farkas Center for Light Induced Processes.

^{b)}Also at The Fritz Haber Center for Molecular Dynamics.

^{c)}Electronic mail: asscher@fh.huji.ac.il

an introduction of the model potential energy surfaces, we shall demonstrate the results of the MD simulations in determining structure, stability, and the dynamical behavior of the adsorbed water clusters. In addition, dimers' diffusion—activation energy determination and their unique diffusion mechanism—will be presented. Finally, TPD spectra were simulated and compared with standard experimental TPD line-shape analysis, as a way to verify the validity of our MD procedure. MD simulations were recently employed²⁴ to study the growth of ice multilayers on a Ru(001)-like surface, suggesting a unique packing geometry of the first four bilayers.²⁴

1. Model potentials and computational procedure

Water molecules were treated as rigid species. This is reasonable since non-dissociative molecular dynamics is of main interest. The interaction between water molecules was calculated using the TIP4P potential.²⁵ The water molecules were kept rigid by the SHAKE/Verlet algorithm.²⁶ Potential cutoff was set at a distance of 14 Å. The time step was 0.968 fs in all the MD runs. The metallic surface potential was adopted from a potential devised by Raghavan *et al.*²⁷ In this potential the metal surface is represented as an effective external periodic field, not as individual atoms. This reduces computation time considerably. This potential was originally developed for Pt(111).²⁷ We have modified it to represent Ru(001) by changing its lattice constant from 2.77 to 2.71 Å, and by increasing the binding energy of water to the substrate by 25%. This difference reflects the experimental data for H₂O on Pt(111) and Ru(001).¹ In order to test the validity of this modification we have used the MD scheme to simulate TPD from the two surfaces, as described in the following. Heating of adsorbed molecules is achieved by randomly distributing velocities among the atoms, and then repeatedly running trajectories for 0.1–1 ps (to allow for structural relaxation) and rescaling the velocities to fit the desired temperature, as defined by the average kinetic energy of the molecules.

2. Clusters formation and stability

The MD simulations based on the potentials described in Sec. II A 1 were utilized in order to examine the formation and relative stability of clusters on the metallic surfaces tested here, Pt and Ru. The most energetically stable configurations of each of the clusters formed are presented in Fig. 1. It appears together with the corresponding calculated dipole moment for an entire cluster, its potential energy, and the energy difference (ΔE) between N water molecules cluster and $N-1$ cluster. Note that the monomer dipole moment is $2.2D$ (Fig. 2) and that its energy on the surface is 2.51 kcal/mol higher than that of the dimer. The energies and dipoles were obtained from averaged values over trajectories of 10 ps, with a “structural snapshot” taken every 0.01 ps. The runs were performed after arranging the molecules at predetermined positions, and heating them to 80 K. One has to examine a major prediction of this work, namely that the large clusters are composed of molecules characterized by a smaller dipole per molecule, therefore contributing less, per molecule, to the measured work function than small clusters.

Dipole Moment [D]	E_{pot} [kcal/mol]		ΔE [kcal/mol]
3.46	-26.34		2.51
3.96	-45.00		6.75
4.71	-61.50		4.59
5.48	-74.80		1.39
5.52	-77.29		3.88
6.53	-96.39		7.19

FIG. 1. The average effective dipoles and potential energies of the most stable configurations of water clusters on Ru(001), as found by MD. On the right are the calculated ΔE values needed to reduce the size of a cluster by 1 water molecule. Note that the dipole moment of a monomer is $2.2D$ (see Fig. 2).

The MD results are shown in Fig. 2. As suggested by the experimental data,⁴ the clustered water molecules are found by the MD simulations to be tilted with respect to the surface normal thus lowering their effective dipole as the cluster size increases, up to a hexamer in our simulations. The monomer in our study adsorbs near perpendicular to the surface on average,^{1,27} in contrast to other calculations that suggested a tilted monomer.²⁸

The calculated potential energies of the clusters provide a reasonable explanation for the relative stability of tetramers.⁶ The extra stability does not arise from the low energy of the tetramer itself, since all the clusters up to hexamers, improve stabilization with the cluster size (see ΔE in Fig. 1). Formation of a tetramer, however, is the least energetic step in the clustering reaction pathway toward hexamer, the building block of a bilayer. A pentamer is most likely formed by adding a monomer to a square tetramer (a gain of 1.39 kcal/mol), followed by ring opening and formation of a

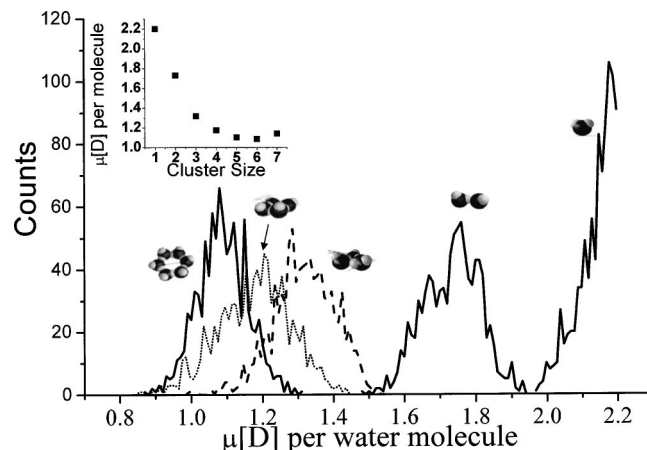


FIG. 2. Histograms of the dipoles per water molecule of different clusters at 80 K averaged over 10 ps runs, snapshot images taken at intervals of 0.01 ps. Inset: The average dipole per water molecule as a function of cluster size.

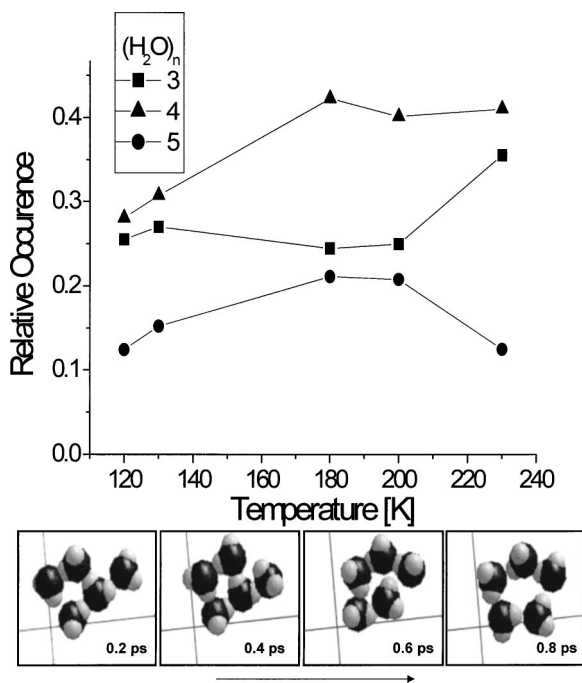


FIG. 3. The relative occurrence ($N_{\text{present}}/N_{\text{total}}$) of tri-, tetra-, and pentamers vs temperature. The surface was covered with six water molecules during a run which was checked every 10 ps for 1.5 ns. Tetramers are the most stable clusters at each temperature. Below: Inclusion of a fifth water molecule into a tetramer shown as snapshots of a MD run every 0.2 ps.

pentamer-pentagon (a gain of 2.49 kcal/mol). This pathway is illustrated in Fig. 3, via 0.2 ps structural snapshots. These are the smallest energy gains among the cluster-forming reactions, or in other words, the pentamer (especially the “square plus one form,” line 4 in Fig. 1) is most likely to undergo dissociation, since the energetic cost for its dissociation is small relative to all other clusters fragmentation reactions.

As supporting evidence, we inferred the relative stability of tetramers from a “dynamical” imaging during the cluster formation process. In order to obtain such images, six water molecules were placed at random on the surface (an equivalent coverage of 3%), heated to different temperatures, and then snapshot imaged along trajectories of 15 ns, counting every 10 ps what cluster sizes were present on the surface. The number of times each cluster was present on the surface (N_{present}) divided by the total number snapshots ($N_{\text{total}} = 1500$) results in the relative occurrence of each cluster size. In order to accelerate the MD runs, we imposed higher temperatures than those used in the experiment in order to increase the effective rates. Each of the trajectories was repeated 10 times per given temperature. The average values are shown in Fig. 3. The results reveal that for temperatures between 120 and 240, the tetramer is the most abundant cluster size, reflecting its extra stability at this temperature range. Summed over the mentioned temperature range cluster abundance ratio (pentamer:tetramer:trimer) was 0.45:1:0.75.

3. Dimer diffusion

Water dimers were reported to diffuse much faster than monomers on Pd(111) employing low temperature STM⁴ at

50 K. This was attributed to their stressed configuration due to mismatch with the surface’s lattice constant. The same trend was found in our MD simulations.²⁹ The diffusion observed with the STM over several seconds was at a surface temperature of 50 K, hence its rate was very slow, a movement of a few lattice sites per second. In order to observe diffusion on the time scale of our simulations, we followed trajectories at a higher temperature range, 110–180 K, and counted the number of jumps each cluster makes during a 3 ns run. These simulations were performed by placing 4 monomers/dimers as far apart as possible on the surface, heating them to the desired temperature, and then snapshot-imaging their motion at 10 ps intervals. Trajectories in which molecules were hopping into contact were eliminated from the final analysis. An Arrhenius plot of $\ln(\text{hops/s})$ versus $1/T$ is shown in Fig. 4. First we used the Pt(111) potential, since its unit cell is closer to the Pd(111) surface used in the STM experiments.⁴ An activation energy for diffusion of 4.2 ± 0.6 kcal/mol was found for monomers, with a prefactor of $10^{15.2 \pm 0.9}$ Hz. Dimers hopped more rapidly on the surface with $E_a = 2.8 \pm 0.2$ kcal/mol and a prefactor of $10^{13.7 \pm 0.4}$ Hz. This prefactor corresponds to a diffusion coefficient of $0.05 \text{ cm}^2/\text{s}$, assuming a hopping distance of one lattice constant. The activation energy for the diffusion of dimers is practically the same as that reported by Mitsui *et al.*⁴ for dimers on Pd(111), (2.9 ± 0.2) kcal/mol. The difference in E_a between monomers and dimers is also quite similar, but the prefactor is an order of magnitude higher in our simulations.

The way our metal lattice is represented via the potential energy surface is not useful for simulating complex electronic interactions. Its strength, however, is in its ability to predict effects that are primarily based on changes in the lattice constant. It was claimed that the fast diffusion of dimers on Pd(111) was due to a misfit between the lattice constant, 2.75 Å, and the O–O distance typical for gas phase water dimers of 2.96 Å. In order to isolate the effect of the lattice, we changed the metal interaction potential by shortening the lattice constant by 7% to 2.6 Å, without changing the interaction strength. We predict that the larger misfit with the smaller lattice constant should increase the hopping speed. This was indeed the result of our MD simulation on such a hypothetical system, as shown in Fig. 4 (circles). The activation energy for diffusion is also significantly reduced in this case to 0.9 ± 0.1 kcal/mol.

The simulations provide a detailed description of the dimers’ hopping mechanism. Figure 5 presents snapshots of several successive configuration changes of a single dimer.²⁹ The dimer is composed of one hydrogen-donor water molecule and one hydrogen-acceptor, according to the hydrogen bond between them. The two water molecules can switch roles, as seen for example between frames 2 and 3 in Fig. 5, but the molecule that hops to another surface site is *always the acceptor*. The donor acts as an anchor while the acceptor hops.

This description offers a unique molecular level insight into the diffusion mechanism of dimers and helps in understanding the surprising result, reported experimentally,⁴ regarding the facile diffusion of dimers.

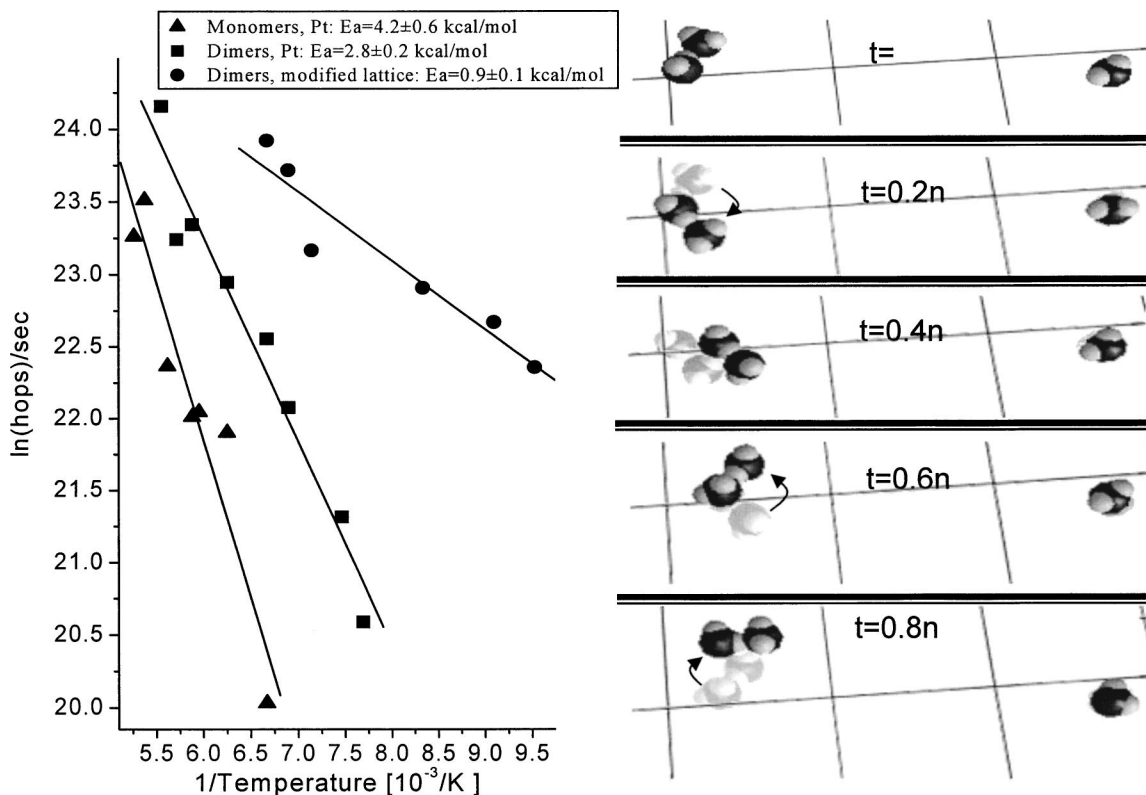


FIG. 4. An Arrhenius plot of hopping rate of monomers and dimers vs inverse temperature on Pt(111). Dimers are plotted also for the case of a Pt(111) surface that was modified to have a lattice constant of 2.6 Å. The number of hops were counted during 2 ns runs. To the right: snapshots of a monomer and a dimer at 180 K. The time between pictures is 200 ps. The dimer is hopping faster than the monomer.

4. MD-TPD

The two metal surfaces (Pt and Ru) were initially covered by 1 BL of water, equivalent to 1.05×10^{15} molecules/cm² on the Ru(001) surface. 180 water molecules were included within the area used for the MD-TPD simulations. The molecules were heated linearly at different heating rates, while monitoring the decreasing coverage every 5 K. The temperature was readjusted every 0.1 ps during the heating ramp. We have excluded the energy contributed by the desorbing molecules to the overall temperature calculation, since the goal was to simulate linear heating of the metallic surface, as in real TPD experiment. Results of a single trajectory are presented in Fig. 6(a). The average of ten such trajectories at a heating rate of 1×10^{12} K/s is shown in Fig. 6(b). The extremely rapid heating rate used here was necessary in order to keep a reasonable computational time for the MD trajectories. The peak desorption rate from Ru(001) is obtained at a higher temperature than the one from Pt(111), as expected experimentally.

The TPD line shape of a typical first-order desorption spectrum is described by the following rate equation:

$$-d\theta/dT = (1/\beta) \cdot \theta \cdot A \exp[-E_{\text{des}}(\theta)/RT], \quad (1)$$

where β is the heating rate, θ the coverage, T the surface temperature, A the first-order frequency factor, E_{des} the activation energy for desorption, and F is a linear correction term for E_{des} due to interactions among neighbor adsorbates. The agreement between the results of the MD simulation and the theoretical line shape is very good and is shown in Fig. 6(b) by a dashed and dotted lines. The parameters used as input for the line shape in the case of Ru(001) were $E_{\text{des}} = 12.5$ kcal/mol, $A = 1.1 \times 10^{14}$ s⁻¹, $F = 1.4$ kcal/mol, and for Pt(111) $E_{\text{des}} = 10$ kcal/mol, $A = 5.5 \times 10^{13}$ s⁻¹, $F = 0.47$ kcal/mol. E_{des} values were set to their known values in the literature.¹

The same MD-TPD simulation and desorption rate equations were repeated at a heating rate of $\beta = 5 \times 10^{12}$ K/s [Fig. 6(c)] using the same parameters as above. The resulting agreement remained the same, demonstrating the consistency and relevance of the MD simulation. For comparison, a TPD measurement at 2K/s is shown in Fig. 6(c) with the calculated line shape predicted by these parameters. The agree-

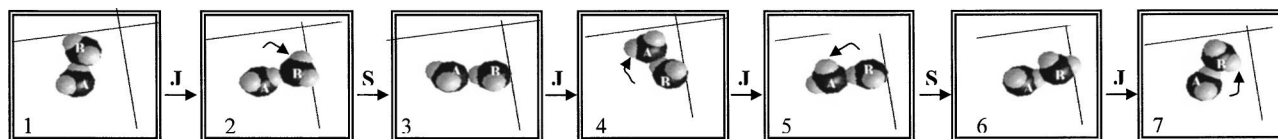


FIG. 5. Snapshots of a dimer during hopping. The two water molecules can switch the donor-acceptor roles (marked as S). Only the acceptor can jump (J) to a near surface site, while the donor remains stationary.

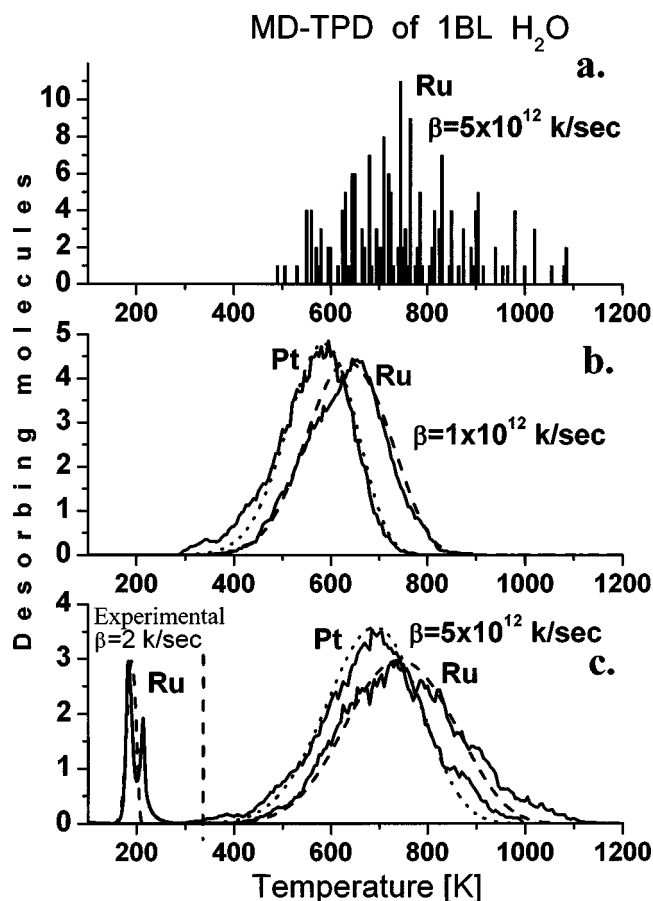


FIG. 6. MD-TPD of 180 water molecules, 1BL, on a surface of an equivalent size of about $40 \times 40 \text{ \AA}$. (a) Nonaveraged, single MD-TPD run. (b) Average of 10 MD-TPD runs for Pt(111) and Ru(001) with a heating rate of $1 \times 10^{12} \text{ K/s}$. (c) Same as (b) for a heating rate of $5 \times 10^{12} \text{ K/s}$. The dashed and dotted lines were calculated using the Arrhenius parameters mentioned in the text.

ment of our MD results with experimental data and simulation indicate that a MD-TPD simulation with a lower heating rate, larger surface area and including moving metal atoms, could provide a realistic description and deeper insight into desorption dynamics. Our scheme differs from previous studies,^{30,31} where MD was employed to extract the activation energy for desorption and the frequency factor, from which a TPD curve could be calculated [using Eq. (1)].

B. Two-dimensional equilibrium model

The nonlinear shape of the work function change ($\Delta\phi$) curve during the initial water adsorption on Ru(001) at 82K (Fig. 7, solid line) was previously explained based on the hypothesis of water cluster formation upon adsorption with decreasing dipole moment per molecule at the larger clusters.⁸ The $\Delta\phi(\theta)$ curve of water was compared to that of CD_3Cl , since CD_3Cl has an identical dipole moment to water at both the gas phase and adsorbed state [on Ru(001)]. In contrast to adsorbed water, however, the methyl chloride molecules repel each other on the surface. This repulsion results in a *linear* decrease of $\Delta\phi$ versus exposure at low coverages, since all the molecules adsorb in a similar environment. In the case of water, the $\Delta\phi$ adsorption curve is

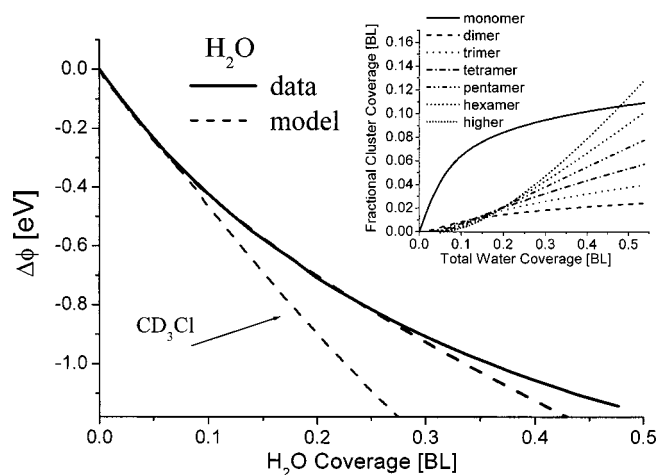


FIG. 7. $\Delta\phi$ during adsorption of H_2O on Ru(001) at 82 K (solid line, see Ref. 8) and the fit of our equilibrium model (dashed). The linear $\Delta\phi$ of $\text{CD}_3\text{Cl}/\text{Ru}(001)$ is shown for comparison. In the inset: the distribution of water molecules among clusters of sizes 1 to 6 as a function of total water coverage. ($i \times N_i$ is plotted vs N_{total} , see the text).

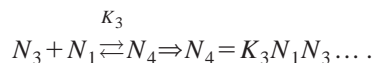
highly nonlinear even at rather low coverages. This behavior has tentatively been associated with cluster formation.⁸ In this section we shall attempt to support this preliminary claim⁸ by employing a simple kinetic model, assuming inter-cluster two-dimensional (2D) “equilibrium” by utilizing the results from the above-described MD simulations.

The effective dipole, μ_{eff} , is defined as the vector component of the molecular dipole moment that is perpendicular to the surface. This dipole contributes to the measured work function change according to the Helmholtz expression $\Delta\phi = -4\pi N\mu_{\text{eff}}$.

The goal of our equilibrium model is to understand the possible effect of clusters on the measured work function with increasing coverage. The model is based on the following assumptions, all were shown to be valid by the MD simulations described earlier: (a) A 2D “equilibrium” is established between clusters of different sizes on the surface, namely, a steady state density of each of the various cluster sizes is assumed. (b) This equilibrium is reached much faster than the rate of adsorption, such that for every coverage there is a unique distribution of clusters. (c) Clusters up to hexamers are explicitly considered as contributing to the measured work function change. In order to simplify the calculations and the model, larger clusters are represented by the formation of heptamers (as seen in Fig. 2, clusters similar or larger than pentamers contribute practically the same effective dipole moment). (d) Each cluster size (i) has a characteristic effective dipole, depending on its geometric configuration, contributing $\Delta\phi_i$ to the total measured work function change.

The coupled equilibrium equations that result from these assumptions are presented in Eq. (2). N_i stands for the surface density of a water cluster of size i :

$$\begin{aligned} K_1 \\ N_1 + N_1 \rightleftharpoons N_2 \Rightarrow N_2 = K_1 N_1^2, \\ K_2 \\ N_2 + N_1 \rightleftharpoons N_3 \Rightarrow N_3 = K_2 N_1 N_2, \end{aligned} \quad (2)$$



An important consequence of Eq. (2) is that the reactions can be divided into two types: between similar species—monomers (K_1) and between a monomer and a cluster (K_2). Thus we set $K_i = K_2$ for $i > 2$. This distinction allows for a significant simplification of the equilibrium equations, although it is not necessarily fully correct. Adding up all N_i results in Eq. (3), expressing the total water coverage:

$$\begin{aligned} N_{\text{total}} &= N_1 + 2N_2 + 3N_3 + 4N_4 + 5N_5 + 6N_6 + 7N_7 \\ &= N_1 + 2K_1 N_1^2 + 3K_2 K_1 N_1^3 + 4K_2^2 K_1 N_1^4 + 5K_2^3 K_1 N_1^5 \\ &\quad + 6K_2^4 K_1 N_1^6 + 7K_2^5 K_1 N_1^7. \end{aligned} \quad (3)$$

Each of the cluster densities N_i is multiplied by its size (i) to get the total number of molecules on the surface— N_{total} . This equation was numerically solved for N_1 for each N_{total} . The larger cluster densities are readily obtained by inserting N_1 into Eq. (2). The total work function change with increasing water coverage is given by

$$\Delta\Phi_{\text{calc}} = \sum_{i=1}^6 N_i \cdot \Delta\Phi_i. \quad (4)$$

The dipoles, μ_i leading to the contribution of each of the clusters ($\Delta\phi_i$) to the overall work function change, were independently obtained from the results of the MD simulations (Sec. II A 2). The curve of $\Delta\phi_{\text{calc}}$ versus coverage was fitted to the measured results, with only K_1 and K_2 remaining as free parameters. The results are shown as the dashed line in Fig. 7. The fit is very good at low coverages, but clearly the model gradually deviates at coverages above 0.35BL since it is no longer correct to limit the clusters to 2D hexamers. Instead, water molecules start forming the hexagonal bilayer network including multilayered three-dimensional islands. A similar limit on the existence of separate clusters, near 0.4BL coverage, was identified in the IRAS analysis.⁶ The “equilibrium” constants derived from our model following a best fit procedure to the experimental data were $K_1 = 1.02\text{BL}^{-1}$ and $K_2 = 9.92\text{BL}^{-1}$.

The insert of Fig. 7 shows the resulting distribution of the water molecules populating the various cluster sizes. This is shown as the fractional coverage of water molecules of a given cluster size relative to a bilayer. In other words, the number of molecules that belong to a specific cluster size— $i \times N_i$ relative to the total number density in a full bilayer, is plotted versus the total water coverage in bilayers. This distribution is consistent with the IRAS measurements,⁶ indicating an initially high coverage of monomers. Our model predicts a non-negligible amount of dimers and trimers, and a significant amount of clusters that are larger than tetramer as coverage increases. These results contradict the interpretations provided based on the IR measurements.⁶

Previous related studies have considered quasiequilibrium or kinetic models to describe similar systems. Wu *et al.*³² developed a model to describe zero-order desorption of H_2O and D_2O from $\text{Ag}(011)$. They assumed a fast equilibrium between monomers and clusters (as in the model described here), followed by desorption of the monomers.

They have used a steady-state approximation for the coverage of monomers, namely assumed $dN_i/dt = 0$. This approximation is not, however, relevant within our model, since their conditions were near the desorption temperature of ice (161 K), while ours is too low (82 K) for desorption to take place. Kasza *et al.*³³ suggested a kinetic model which is governed by irreversible nucleation, instead of an equilibrium state. They attempted to use their model to follow the IR absorbance of water on $\text{Al}(001)$, predicting a strong dependence on the flux of adsorbing molecules. Their model, however, failed to fit their own data, perhaps due to the irreversibility assumption rather than equilibrium.

We have measured the $\Delta\Phi$ response at different pressures, resulting in an order of magnitude difference in flux, but could not observe any change in the $\Delta\Phi$ versus coverage curve on $\text{Ru}(001)$ at 82 K.

III. CONCLUSIONS

Structure and effective dipoles of small water clusters on $\text{Ru}(001)$ were determined using MD simulations. A possible explanation for the relative stability of tetramers at low coverages was presented by analyzing the energies of the different cluster sizes obtained from the MD simulations. High abundance and stability of tetramers was obtained directly from the MD simulations of the water clusters at an effective coverage of 3%. Fast diffusion of dimers measured by STM was reproduced in our simulations. The activation energy for diffusion of dimers was found to be 2.8 ± 0.2 kcal/mol with a prefactor of $10^{13.7 \pm 0.4}$ Hz. A 7% decrease in the lattice constant resulted in a 70% decrease in the activation energy for diffusion, supporting the prediction of our model that the diffusion is assisted by a mismatch between cluster structure and the surface lattice distance. A novel diffusion mechanism of dimers on metal surfaces has been proposed.

Finally, the dipole moments extracted from the MD scheme, were utilized as input for an equilibrium model that described the coverage dependent surface work function change. This model fits the $\Delta\phi$ data up to a coverage of 0.35BL, predicting an order of magnitude larger equilibrium constant for association of water to form large clusters than for the formation of dimers from monomers.

ACKNOWLEDGMENTS

This work was partially supported by a grant from the U.S.–Israel Binational Foundation and the Israel Science Foundation. The Farkas center is supported by the Bundesministerium für Forschung und Technologie and the Minerva Gesellschaft für die Forschung mbh.

¹P. A. Thiel and T. E. Madey, *Surf. Sci. Rep.* **7**, 211 (1987).

²M. A. Henderson, *Surf. Sci. Rep.* **285**, 1 (2002).

³K. Jacobi, K. Bedurftig, Y. Wang, and G. Ertl, *Surf. Sci.* **472**, 9 (2001).

⁴T. Mitsui, M. K. Rose, E. Fomin, D. F. Ogletree, and M. Salmeron, *Science* **297**, 1850 (2002).

⁵K. Morgenstern and J. Nieminen, *Phys. Rev. Lett.* **88**, 066102 (2002).

⁶(a) M. Nakamura and M. Ito, *Chem. Phys. Lett.* **325**, 293 (2000); (b) M. Nakamura, Y. Shingaya, and M. Ito, *ibid.* **309**, 123 (1999).

⁷A. L. Glebov, A. P. Graham, and A. Menzel, *Surf. Sci.* **427**, 22 (1999).

⁸Y. Lilach, L. Romm, T. Livneh, and M. Asscher, *J. Phys. Chem. B* **105**, 2736 (2001).

- ⁹D. L. Doering and T. E. Madey, *Surf. Sci.* **123**, 305 (1982).
- ¹⁰J. D. Bernal and R. H. Fowler, *J. Chem. Phys.* **1**, 515 (1933).
- ¹¹L. Pauling, *J. Am. Chem. Soc.* **57**, 2680 (1935).
- ¹²G. Held and D. Menzel, *Surf. Sci.* **316**, 92 (1994).
- ¹³G. Held and D. Menzel, *Phys. Rev. Lett.* **74**, 4221 (1995).
- ¹⁴P. J. Schmitz, J. A. Polta, S.-L. Chang, and P. A. Thiel, *Surf. Sci.* **186**, 219 (1987).
- ¹⁵P. A. Thiel, F. M. Hoffman, and H. Weinberg, *J. Chem. Phys.* **75**, 5556 (1981).
- ¹⁶P. J. Feibelman, *Science* **295**, 99 (2002).
- ¹⁷C. J. Tsai and K. D. Jordan, *J. Phys. Chem.* **97**, 11227 (1993).
- ¹⁸S. S. Xantheas and T. H. Dunning, Jr., *J. Chem. Phys.* **99**, 8774 (1993).
- ¹⁹J. M. Pedulla, K. Kim, and K. D. Jordan, *Chem. Phys. Lett.* **291**, 78 (1998).
- ²⁰K. Kim, K. D. Jordan, and T. S. Zwier, *J. Am. Chem. Soc.* **116**, 11568 (1994).
- ²¹M. Severson and V. Buch, *J. Chem. Phys.* **111**, 10866 (1999).
- ²²M. G. Brown, F. N. Keutsch, and R. J. Saykally, *J. Chem. Phys.* **109**, 9645 (1998).
- ²³K. Karapetian and K. D. Jordan, in *Water in Confined Environments*, edited by J. P. Devlin and V. Buch (Springer, New York, in press), pp. 4–7.
- ²⁴H. Witek and V. Buch, *J. Chem. Phys.* **110**, 3168 (1999).
- ²⁵W. L. Jorgensen, J. Chandrasekhar, J. D. Madura, R. W. Impey, and M. L. Klein, *J. Chem. Phys.* **79**, 926 (1983).
- ²⁶S. Kuwajima and A. Warshel, *J. Phys. Chem.* **94**, 460 (1990).
- ²⁷K. Raghavan, K. Foster, K. Motakabbir, and M. Berkowitz, *J. Chem. Phys.* **94**, 2110 (1991).
- ²⁸J. E. Muller, *Physics and Chemistry of Alkali Metal Adsorption*, edited by H. P. Bonzel, A. M. Bradshaw, and G. Ertl (1989), p. 271.
- ²⁹An animation of our MD results can be seen in <http://chem.ch.huji.ac.il/Cluster.html>. See directions there.
- ³⁰A. P. J. Jansen, *J. Chem. Phys.* **97**, 5205 (1992).
- ³¹K. A. Fichthorn and R. A. Miron, *Phys. Rev. Lett.* **89**, 196103 (2002).
- ³²K. J. Wu, L. D. Peterson, G. S. Elliott, and S. D. Kevan, *J. Chem. Phys.* **91**, 7964 (1989).
- ³³R. V. Kasza, K. Griffiths, V. P. Zhdanov, and P. R. Norton, *Appl. Surf. Sci.* **84**, 97 (1995).